Analytical wavefront curvature correction to the weak-contrast AVO approximation

for a plane reflector

Badr Alulaiw[1] and Boris Gurevich[2,3]

Right-running Head: **Wavefront curvature correction for AVO**

[1]*Formerly Curtin University of Technology, Department of Exploration Geophysics; presently Saudi Aramco, Dhahran, Saudi Arabia. E-mail: badr.ulaiw@aramco.com .*

[2]*Curtin University, Department of Exploration Geophysics, GPO Box U1987, Perth, WA 6845, Australia E-mail: B.Gurevich@curtin.edu.au .*

[3]*CSIRO Earth Science and Resource Engineering, ARRC, 26 Dick Perry Avenue, Kensington, Perth, WA 6151, Australia.*

ABSTRACT

Most amplitude versus offset (AVO) analysis and inversion techniques are based on the Zoeppritz equations for plane-wave reflection coefficients or their approximations. Real seismic surveys use localized sources that produce spherical waves, rather than plane waves. In the far field, the AVO response for a spherical wave reflected from a plane interface can be well approximated by a plane-wave response. However this approximation breaks down in the vicinity of the critical angle. Conventional AVO analysis ignores this problem and always utilises the plane-wave response. This approach is sufficiently accurate as long as the angles of incidence are much smaller than the critical angle. Such moderate angles are more than sufficient for the standard estimation of AVO intercept and gradient. However, when independent estimation of the density is required, it may be important to use large incidence angles close to the critical angle, where spherical wave effects become important. For the amplitude of a spherical wave reflected from a plane fluid-fluid interface, an analytical approximation is known, which provides a correction to the plane-wave reflection coefficients for all angles. For the amplitude of a spherical wave reflected from a solid/solid interface, we propose a formula which combines this analytical approximation with the linearised plane-wave AVO equation. The proposed approximation shows reasonable agreement with numerical simulations for a range of frequencies. Using this solution, we constructed a two-layer three-parameter least-squares inversion algorithm. Application of this algorithm to synthetic data for a single interface shows an improvement compared to the use of plane-wave reflection coefficients.

KEYWORDS

INTRODUCTION

Most AVO analysis and inversion techniques are based on the Zoeppritz equations for plane-wave reflection coefficients or their approximations. Real seismic surveys use localized sources that produce spherical waves, rather than plane waves. AVO response for a spherical wave reflected from a plane interface differs from that for a plane wave, especially for angles close to or beyond the critical angle (Červený 1961; Červený and Ravindra 1971; Krail and Brysk 1983; Winterstein and Hanten 1985; Alhussain et al. 2008; Skopintseva et al., 2009).

There are some important differences between plane and spherical waves. First, amplitude of a spherical wave varies with the distance from the source, whereas the amplitude of a plane wave in a homogeneous medium is constant. The amplitude decay for spherical waves is called geometrical spreading and its effect can be accounted for. Second, a spherical wave can be seen as an integral over a range of plane-waves with different ray parameters and directions. Third, the response of a spherical wave depends on the frequency content of the seismic wave (Ursenbach et. al. 2007).

Figure 1 shows real part of reflection coefficients versus angle of incidence (AVA curves) computed using the Zoeppritz equations, Thomsen approximation and the exact numerical solution for Model A shown in Table 1. The amplitudes extracted from the numerical solution were corrected for geometrical spreading. The critical angle for this model is 56.44˚. At least three observations can be made from this figure. First, AVO curves of the plane-wave exact solution and its approximation coincide with those of a full elastic wave at angles well below the critical angle. Second, AVO responses of the plane wave and its

approximation deviate significantly from the response of the full elastic wave at the vicinity of the critical angle. Finally, the full elastic responses are frequency dependent.

It was shown by Alhussain et al. (2008) that the AVO inversion for two parameters (P-wave and S-waves impedance) using the Zoeppritz equations over short offset is robust. However, inversion for three parameters (density ρ, P-wave velocity V_P and S-wave velocity V_S) is unstable and the results depend on the frequency at wide angles. Downton and Ursenbach (2006) showed that use of the critical angle improves accuracy of the computed densities for inversions using the Zoeppritz equations.

Recently, Ursenbach et al. (2007) developed an approach that accounts for the spherical wave AVO effects. Unlike the Zoeppritz equations for plane waves, the reflected amplitude for spherical waves is represented by a double integral over frequency and wavenumber. For scalar potential of the PP reflected wave, the wavenumber integral has the form (Aki and Richards 1980)

$$\phi(\omega) = Ai\omega e^{(-i\omega t)} \int_0^\infty R \frac{p}{\zeta} J_0(\omega px) e^{-i\omega\xi(z+h)} dp . \tag{1}$$

In equation (1), A is a scaling factor, ω is the frequency, t is the time, p is the horizontal slowness, ζ is the vertical P-wave slowness in the upper layer, R is the plane-wave PP reflection coefficient, J_0 is the zero-order Bessel function, x is the horizontal receiver coordinate (source-receiver offset), h and z are the vertical coordinates of the source and receiver, respectively (the interface is assumed to be a $z=0$ plane). In order to obtain the displacement from this equation, a gradient with respect to the receiver position is computed

and weighted by the wavelet. Finally, an inverse Fourier transform is performed. These steps yield the displacement time trace observed at the receiver, from which we can extract AVO information (Haase 2004; Ursenbach et. al. 2005).

Spherical wave AVO inversion requires these computations to be repeated multiple times in an iterative fashion, making the procedure computationally expensive. Ursenbach et al. (2007) simplified these computations by using an analytical form of the source wavelet, which allows integration over the frequency to be done analytically and numerical integration over the wavenumber to be optimised.

An alternative approach is to use analytical approximation for the reflection coefficient for spherical waves. Such an approximation can be obtained from a high-frequency asymptotic expansion of the integral in equation (1). The leading (zero-order) term in this asymptotic approximation for the amplitude of a reflected spherical wave can be written as $R(\theta)/r$ where R is the plane-wave reflection coefficient for an incidence angle θ and r is the length of the ray path from the source to the receiver. The next (first-order) approximation can be written as $R(\theta)\left(1/r + B(\theta)/kr^2\right)$, where k is the characteristic wavenumber and B is a dimensionless quantity of order 1 (Červený and Ravindra 1971; Brekhovskikh and Godin 1999). For typical situations in petroleum seismology, P-wave velocity $V_P > 3$ km/s, central frequency $f > 30$ Hz and $r > 2$ km, so that $kr = 2\pi f r / V_P > 120$. Thus, the term $B(\theta)/kr^2$ is less than 0.01 of the zero-order term $1/r$. This means that the zero-order approximation $R(\theta)/r$ is very accurate and the first-order corrections are only important for near-surface applications.

However, numerical simulations and theoretical analysis show that the ray theory approximations described above break down in the vicinity of the critical angle. Furthermore, in the vicinity of the critical angle, the spherical wave correction is of the order $(kr)^{-1/4}$, and therefore is important for much larger values of kr than the first-order correction $B(kr)^{-1}$ (Červený and Ravindra 1971; Brekhovskikh and Godin 1999). The behavior of the spherical-wave reflection coefficients in the vicinity of the critical angle was analysed by Červený (1961), who proposed an analytical approximation to account for these effects. In this approximation, the reflection coefficients below and above the critical angle are described by two different expressions. A more compact form of this approximation for a fluid/fluid interface was proposed in Brekhovskikh and Godin (1999). In this paper we propose a heuristic extension of the latter approximation to solid/solid interfaces and explore its applicability to long-offset AVO analysis.

First, we describe an analytical approximation for a spherical-wave reflection coefficient for a plane fluid/fluid interface. Then, for a solid/solid interface, we combine this approximation with a weak-contrast approximation for plane-wave reflection coefficients. The combined approximation for the solid case is then computed for a number of models and compared with the numerical solution. Finally, using this solution, we construct a two-layer, three-parameter, least-squares inversion algorithm and demonstrate its performance using a simple synthetic example.

Our analysis is limited to reflection from a plane interface between two homogeneous and isotropic solids. Another factor that may complicate AVO analysis is the curvature of the interface itself (Ayzenberg et al., 2009; Skopintseva et al.; 2010). Analysis of this effect is beyond the scope of the present paper.

ANALYTICAL EXPRESSION FOR A FLUID/FLUID INTERFACE

Brekhovskikh and Godin (1999) showed that the reflection coefficient for a spherical wave reflected from an interface between two fluids with sound velocities V_{P1} and V_{P2} and densities ρ_1 and ρ_2 can be approximated as a sum

$$R_f(\theta) = V_1 + p_2,\qquad (2)$$

where the regular part V_1 of the reflection coefficient is given by

$$V_1 = \frac{m^2 + n^2 - (m^2 + 1)q^2}{m^2 - n^2 - (m^2 + 1)q^2}\qquad (3)$$

with $m = \rho_2/\rho_1$, $n = V_{P1}/V_{P2}$ and $q = \sin\theta$. In turn, the 'singular' part p_2 (the part with a singularity at the critical angle in the high-frequency limit) is

$$p_2 = \frac{2^{3/2}\sin\delta\exp\left[ikR_1\left(\frac{\cos(\theta-\delta)}{2}\right)^2 - \frac{7i\pi}{8}\right]}{m(kR_1)^{\frac{1}{4}}\left[\sin\theta\cos\delta\left(\cos\left(\frac{(\theta-\delta)}{2}\right)\right)^3\right]^{\frac{1}{2}}} \times \frac{\left[D_{\frac{1}{2}}(u) + \frac{A-1}{u}D_{\frac{3}{2}}(u)\right]}{\exp(ikR_1)},\qquad (4)$$

where θ is the angle of incidence, δ is the critical angle, k is the wavenumber in the upper layer, R_1 is the distance between the image source in the lower layer and the receiver, and

$D_{\frac{1}{2}}$ and $D_{\frac{3}{2}}$ are parabolic cylinder functions (Abramowitz and Stegun 1965; Olver et al. 2010; Daley 2001). Quantities u and A are given by

$$u = 2\exp\left(3\pi i/4\right)\left(kR_1\right)^{\frac{1}{2}}\sin\left(\frac{\theta-\delta}{2}\right) \tag{5}$$

and

$$A = \frac{m^2\left[0.5\sin\theta\cos\delta\sin\left(\theta+\delta\right)\right]^{\frac{1}{2}}\cos\theta\left(\cos\frac{\left(\theta-\delta\right)}{2}\right)^2}{\sin\delta\left(m^2\left(\cos\theta\right)^2+\left(\sin\theta\right)^2-\left(\sin\delta\right)^2\right)}. \tag{6}$$

Figure 2 shows the real part of reflection coefficient versus the incidence angle curves obtained from synthetic seismograms for an acoustic wave reflected from a single interface between two fluids with sound velocities $V_{P1}=1500$ m/s and $V_{P2}=2000$ m/s, and densities $\rho_1=1$ g/cm^3 and $\rho_2=2$ g/cm^3. The point source and receiver were 500 m above the reflector and the source wavelet was the Ricker wavelet with central frequency of 50 Hz. The seismograms were computed using Kennett's reflectivity method (Kennett 1979) and then corrected for normal moveout (NMO) using known overburden velocity V_{P1} and for geometrical spreading. Then, the amplitude on the zero offset trace was picked at the time T_0 of the maximum of the wavelet. On all other traces the amplitude (total displacement) was picked at the same time T_0 (since after NMO correction the reflected waves are supposed to have the same arrival times on all traces). It is shown in Appendix A that the amplitudes so picked correspond to the real part of the complex reflection coefficient. Also shown are the real parts of the plane wave reflection coefficient and of the spherical wave approximation

computed with equations (2)-(6). We see that the spherical correction greatly improves the match with the synthetic amplitude versus angle (AVA) curve around the critical angle.

ANALYTICAL APPROXIMATION FOR A SOLID/SOLID INTERFACE

Analytical expressions 2-6 are for a fluid/fluid interface, and thus are not particularly useful for practical AVO analysis in geologic media. Similar expressions for a solid/solid interface are known, but the expressions are very complicated (Červený 1961). Alternatively, we can try to adopt a curvature correction to a linearised approximation widely used for plane-wave AVO.

In case of small contrasts between properties of two solid media, the PP plane-wave reflection coefficient for an interface between these media can be written as (Aki and Richards, 1980; Thomsen, 1990)

$$R(\theta) = \frac{1}{2}\frac{\Delta Z}{\overline{Z}} + \frac{1}{2}\left\{\frac{\Delta V_\mathrm{P}}{\overline{V}_\mathrm{P}} - \left(\frac{2\overline{V}_\mathrm{S}}{\overline{V}_\mathrm{P}}\right)^2 \frac{\Delta G}{\overline{G}}\right\}\sin^2\theta + \frac{1}{2}\frac{\Delta V_\mathrm{P}}{\overline{V}_\mathrm{P}}\sin^2\theta\tan^2\theta \,, \tag{7}$$

where Z denotes acoustic impedance, $G = \rho V_\mathrm{S}^2$ is the shear modulus, θ the is average of the incidence angle and the refraction angle, and $\dfrac{\Delta x}{\overline{x}}$ denotes relative contrast in the property x between the media 1 and 2. Equation (7) can be rewritten in the form

$$R(\theta) = R_f(\theta) - \frac{1}{2}\left(\frac{2\overline{V}_\mathrm{S}}{\overline{V}_\mathrm{P}}\right)^2 \frac{\Delta G}{\overline{G}}\sin^2\theta \,, \tag{8}$$

where $R_f(\theta)$ is the linearized approximation for the plane-wave reflection coefficient from an interface between two fluids with the same *P*-wave velocities and densities as in the two solid layers (see e.g., Chapman 2010). To account for the wavefront curvature, we propose to replace the plane wave coefficient for a fluid/fluid interface, $R_f(\theta)$, with the spherical wave reflection coefficient given by equation (2),

$$R(\theta) = V_1 + p_2 - \frac{1}{2}\left(\frac{2\overline{V}_S}{\overline{V}_P}\right)^2 \frac{\Delta G}{\overline{G}}(\sin\theta)^2 \qquad (9)$$

with V_1 and p_2 given by equations (3) and (4), respectively.

Equation (9) is our new heuristic approximation. By construction, it coincides with the Brekhovskikh-Godin approximation for a fluid/fluid case, and with the plane-wave lineraised AVO approximation in the far-field limit. In other cases it requires numerical testing to determine its accuracy, To this end, AVO curves were extracted from synthetic seismograms (computed by the reflectivity method) for various models shown in Table 1 using the Ricker wavelet with frequencies of 30Hz, 50 Hz and 80Hz, at a depth of 500 m. Corresponding AVO curves were also computed using the plane-wave Zoeppritz equations and the Thomsen (1990) approximation, equation (7) and our proposed spherical wave approximation, equation (9). Figure 3 a-g shows the real part of the reflection coefficient along with the real part of the amplitude obtained from synthetic seismograms. Provided the contrasts in elastic parameters between upper and lower layers are small, our approximation is in a good agreement with synthetic data. When the contrast between the two media is large, the quality of the approximation deteriorates. To be more specific, our approximation provides very good results even if the contrast in V_P is large. When the contrast in V_S is large, however, Zoeppritz equations provide better results in near offset. This is expected as our approximation is based on the Thomsen approximation, which is only valid for small contrast. Hence, the inversion

results using the proposed method are expected to be the same or better than those based on the linearised Zoeppritz equations. Importantly, the inversion will not be limited to the data below the critical angle.

One can also observe from Figures 3 (a-i) that our approximation produces slight oscillations of the reflection coefficient with angle in the post-critical domain. This phenomenon has been nicely examined by Červený (1961), who showed these oscillations are the result of the interference of the post-critical reflected wave (in the narrow sense of the word) with the refracted wave (see also Ayzenberg et al. 2009). Our numerical data, however, do not appear to show any oscillations. As noted by Skopintseva et al. (2010), this may be the result of the fact that the numerical modelling was done for a pulse containing a range of frequencies, rather than a single frequency. Since seismic exploration is performed using narrow-band signals (no more than one decade in frequency), our single-frequency approximation is still adequate and constitutes an improvement over the use of plane-wave reflection coefficients, which correspond to the infinite frequency limit of the spherical-wave reflection coefficient. However our approximation is only valid as long as the two events form an interference pattern (Červený 1961).

INVERSION EXAMPLE FOR A SINGLE PLANE INTERFACE

It is clear from many earlier studies (Červený and Ravindra 1971; Ursenbach et al. 2007; Alhussain et al. 2008; Ayzenberg et al. 2009) as well as from our examples that the spherical wavefront curvature effects are only important at long offsets, close to or beyond the critical angle. These large angles are unnecessary for standard two-parameter AVO analyses, but may be important for three-parameter inversions, when independent recovery of P- and S-

wave velocities and density is desired (Lines 1999; Li 2005; Downton and Chaveste 2004). To test how our approximation performs for this purpose, we have developed a simple least-squares three-parameter non-linear inversion procedure for a single plane interface. The algorithm (similar to the one described by Alhussain et al. 2008) assumes that the properties of the upper layer (medium 1) are known, and attempts to find the properties of the bottom layer (medium 2). The algorithm attempts to estimate P- and S-wave velocities and density of medium 2 by fitting the AVA curve extracted from our 50 Hz synthetic data for Model A (Table 1) using the exact Zoeppritz equations, Thomsen's approximation and the spherical wave approximation, equation (9).

The inversion is based on an unconstrained nonlinear optimisation that starts from an initial model and then tries to find the minimum of a scalar function of several variables. This optimisation utilises the Nelder-Mead simplex algorithm developed by Lagarias et al (1998) and implemented in Matlab. We use this algorithm to find elastic parameters of the lower layer such that the difference between the synthetic AVO curve and the AVO curve computed by our approximation is the minimum. The errors in estimated parameters were computed using the equation

$$Error(\%) = \frac{\left|Actual\_Value - Inverted\_Value\right|}{Actual\_Value} * 100 . \tag{10}$$

The percent error in estimating V_{P2}, V_{S2} and ρ_2 as a function of the offset range is shown in Figure 4 for noise-free data. Figure 5 shows the same result but for the case where random noise was added to the seismograms before extracting the amplitudes (the signal-to-noise ratio was 2). We see that for the noise-free data all the algorithms provide accurate

estimations of all elastic parameters, and moderate angles (below 45 degrees) give best results. The use of a broader offset range increases the error in the inversion based on Zoeppritz equations and their linearised approximation due to the distorting effect of wavefront curvature. However, in the presence of noise, use of a limited offset range results in large random errors and the use of long offsets becomes important. For those large offsets and angles, the use of plane wave reflection coefficients results in systematic errors due to wavefront curvature effects. In these cases our spherical curvature approximation provides a more accurate and robust inversion result.

CONCLUSIONS

For three-parameter AVO inversion it may be beneficial to use angles close to the critical angle, where spherical wave effects become important. These effects can be taken into account using a known asymptotic approximation based on parabolic cylinder functions. This approximation has a relatively simple form for a plane fluid-fluid interface. For a plane solid-solid interface, we have proposed a heuristic formula that combines this known acoustic approximation with the low-contrast (linearised) plane-wave AVO equation. Predictions of this heuristic approximation show a reasonable agreement with numerical simulations when the S-wave velocity contrast between the two media is not too large. Use of this solution in an iterative two-layer, 3-parameter inversion for a single plane interface gives more robust estimates than the standard plane-wave AVO inversion algorithm.

References

Abramowitz, M., and Stegun, I. A. 1965. Handbook of Mathematical Functions. Dover.

Aki, K., and Richards, P. G.. 1980. Quantitative seismology: theory and methods. W. H. Freeman and Company.

Alhussain, M., Gurevich, B., and Urosevic, M. 2008. Experimental verification of spherical-wave effect on the AVO response and implications for three-term inversion. *Geophysics* **73**, C7-C12.

Ayzenberg, M., Tsvankin, I., Aizenberg, A., and Ursin, B. 2009. Effective reflection coefficients for curved interfaces in transversely isotropic media. *Geophysics* **74**, WB33–WB53, 10.1190/1.3197862.

Brekhovskikh, L. M., and Godin, O. A. 1999. Acoustics of Layered Media II. Point Sources and Buondary Beams. Springer.

Červený,V. 1961. The amplitude curves of reflected harmonic waves around the critical point. Studia Geophysica et Geodaetica **5**, 319–351.

Červený,V., and Ravindra, R. 1971. Theory of Seismic Head Waves. University of Toronto Press.

Chapman, C. 2010. Fundamentals of Seismic Wave Propagation. Cambridge University Press.

Daley, P.F. 2001. The parabolic cylinder function in elastodynamic problems. CREWES
  Research Report, Vol. 13, 181-185.

Downton, J. and Chaveste, A. 2004. Calibrated three-term AVO to estimate density and water
  saturation. Canadian Society of Exploration Geophysicists, Extended Abstract

Downton, J. E. and Ursenbach, C. 2006. Linearized amplitude variation with offset (AVO)
  inversion with supercritical angles. Geophysics **71**, E49-E55.

Haase, A. B. 2004. Spherical wave AVO modeling of converted waves in isotropic media.
  SEG Technical Program Expanded Abstracts **23**, 263-266.

Kennett, B. L. N. 1979. Theoretical reflection seismograms for an elastic medium.
  Geophysical Prospecting **27**, 301–321.

Krail, P. M., and Brysk, H. 1983. Reflection of spherical seismic waves in elastic layered
  media. Geophysics 48, 655-664.

Lagarias, J. C., Reeds J. A., Wright M. H., and Wright P. E. 1998. Convergence Properties of
  the Nelder-Mead Simplex Method in Low Dimensions. SIAM Journal of
  Optimization 9, no. 1,112–147.

Li, Y. 2005. A study on applicability of density inversion in defining reservoirs. 75th Annual
  International Meeting, SEG, Expanded Abstracts 24, 1646-1649.

Lines, L. 1999. Density and AVO. Canadian Journal of Exploration Geophysics **35**, 32-35.

Olver, F.W. J., Lozier , D. W., Boisvert, R.F., and Clark, C.W. eds. 2010. NIST Handbook of
  Mathematical Functions. Cambridge University Press.

Skopintseva, L.V. Ayzenberg, M.A., Landrø, M., and Nefedkina, T.V. and Aizenberg, A.M.,
  2009, Testing the Performance of AVO Inversion Based on Effective Reflection
  Coefficients on Long-offset Synthetic PP Data, 71nd EAGE Conference &
  Exhibition, Extended Abstract.

Skopintseva, L.V. Aizenberg, A.M., Ayzenberg, M.A., Landrø, M., and Nefedkina, T.V. 2010. Applicability of AVO inversion based on effective reflection coefficients to long-offset data from curved interfaces. 72nd EAGE Conference & Exhibition, Extended Abstract.

Thomsen, L. 1990. Poisson was not a geophysicist!. The Leading Edge **9**, 27-29.

Ursenbach, C., Haase A. B., and Downton J. E.. 2005. An efficient method for AVO modeling of reflected spherical waves. SEG Technical Program Expanded Abstracts **24**, 202-205.

Ursenbach, C. P., Haase A. B., and Downton J. E. 2007. Efficient spherical-wave AVO modeling. The Leading Edge **26**, 1584-1589.

Winterstein, D. F., and Hanten J. B.. 1985. Supercritical reflections observed in P- and S-wave data. Geophysics **50**, 185-195.

Appendix A.

Let $f(t)$ be a real and symmetric incident wavelet, and $F(\omega)$ its Fourier transform (FT). If $f(t)$ is symmetric about time $t = 0$ (zero-phase) then $F(\omega)$ is real and symmetric. Let $R(\omega) = A(\omega) + iB(\omega)$ be the complex and frequency-dependent reflection coefficient at a given angle of incidence. Note that since the reflected signal is the convolution of the incident wavelet with the inverse Fourier transform (FT^{-1}) of the reflection coefficient, $FT^{-1}\{R(\omega)\}$ must be real. It follows that $A(\omega)$ must be symmetric and $B(\omega)$ antisymmetric functions of ω. Then, the Fourier transform of the reflected wave is

$$G(\omega) = R(\omega)F(\omega) = A(\omega)F(\omega) + iB(\omega)F(\omega). \tag{A1}$$

Then the reflected wave in the time domain $g(t)$ is the inverse Fourier transform of $G(\omega)$,

$$g(t) = FT^{-1}\{G(\omega)\} = FT^{-1}\{R(\omega)F(\omega)\} = a(t) + b(t) \tag{A2}$$

where $a(t) = FT^{-1}\{A(\omega)F(\omega)\}$ and $b(t) = FT^{-1}\{iB(\omega)F(\omega)\}$.

Note that since $A(\omega)$ is real, its inverse Fourier transform $a(t)$ is symmetric (even function). At the same time, $iB(\omega)$ is pure imaginary, and thus $b(t)$ is antisymmetric (odd function) about time $t = 0$. Therefore, $b(0) = 0$ and

$$g(0) = a(0) = FT^{-1}\{A(\omega)F(\omega)\}\big|_{t=0} = \frac{1}{2\pi}\int_{-\infty}^{\infty} A(\omega)F(\omega)\,d\omega. \tag{A3}$$

Thus, the amplitude of the reflected wave at $t = 0$ is defined by $A(\omega)$, the real part of $R(\omega)$. Furthermore, if $A(\omega)$ does not vary very much within the frequency range of the wavelet, then within this range we can approximate it by its value at the central frequency of the wavelet ω_c, $A(\omega) \equiv A(\omega_c)$, so that

$$g(0) = \frac{A(\omega_c)}{2\pi}\int_{-\infty}^{\infty} F(\omega)d\omega = A(\omega_c)f(0). \tag{A3}$$

Thus the amplitude of the reflected wave at $t = 0$ equals the amplitude of the incident wave times the real part of the reflection coefficient at the central frequency of the wavelet.

Note that this analysis rests on three assumptions: 1) the wavelet is zero-phase, 2) the event is picked at zero time (i.e, the time of the maximum at zero offset after NMO), and 3) the real part of the reflection coefficient does not vary very much within the frequency range of the wavelet.

To obtain the absolute value of the reflection coefficient from seismograms, we must pick the maximum of the envelope. Comparison of this maximum against the absolute values of the plane-wave and spherical-wave approximations is shown in Figure 6 (for Model A). One can again see a reasonable agreement between the numerical results and our heuristic approximation, equation (9).

TABLE HEADINGS

Table 1: Properties of two solid media in the synthetic models.

Table 1: Properties of two solid media in the synthetic models.

	Depth (m)		Vp (m/s)	Vs(m/s)	Density (g/cm^3)
Model A	500	Upper Layer	2500	1200	2.00
		Lower Layer	3000	1300	2.20
Model B	500	Upper Layer	2000	1200	2.00
		Lower Layer	3000	1300	2.20
Model C	500	Upper Layer	1500	1200	2.00
		Lower Layer	3000	1300	2.20
Model D	500	Upper Layer	2500	1200	2.00
		Lower Layer	3000	1700	2.20
Model E	500	Upper Layer	2500	1200	2.00
		Lower Layer	3000	2000	2.20
Model F	500	Upper Layer	2500	900	2.00
		Lower Layer	3000	1300	2.20
Model G	500	Upper Layer	2500	1500	2.00
		Lower Layer	3000	1300	2.20
Model H	1000	Upper Layer	2500	1200	2.00
		Lower Layer	3000	1300	2.20
Model I	1500	Upper Layer	2500	1200	2.00
		Lower Layer	3000	1300	2.20

FIGURE CAPTIONS

Figure 1. Real Components of reflection coefficientscomputed using the Zoeppritz equations, Thomsen approximation and full elastic Model A with parameters shown in Table 1. Note the discrepancy in AVO response in the vicinity of critical angle. Also, note the frequency dependence of spherical wave responses.

Figure 2. Comparison of real components of reflection coefficients computed from synthetic data (blue), Zoeppritz equations (black) and the spherical wave analytical solution at the fluid-fluid interface (red).

Figure 3. Comparison of real components of reflection coefficients computed from synthetic data, and given by the Zoeppritz equations, Thomsen's linearised approximation, and the proposed spherical wave approximation at an interface between two media with parameters corresponding to Models A-I (Table 1).

Figure 4. Error in estimating V_{P2} (a), V_{S2} (b), and ρ_2 (c) in 3-parameter inversion of synthetic angle dependent reflectivity (d).

Figure 5. Error in estimating V_{P2} (a), V_{S2} (b), and ρ_2 (c) in 3-parameter inversion of synthetic angle dependent reflectivity with 50% added white noise (d).

Figure 6. Same as Figure 3a but for absolute values of the reflection coefficients. 'Synthetic' refers to amplitude of the envelope of the reflected wavelet.
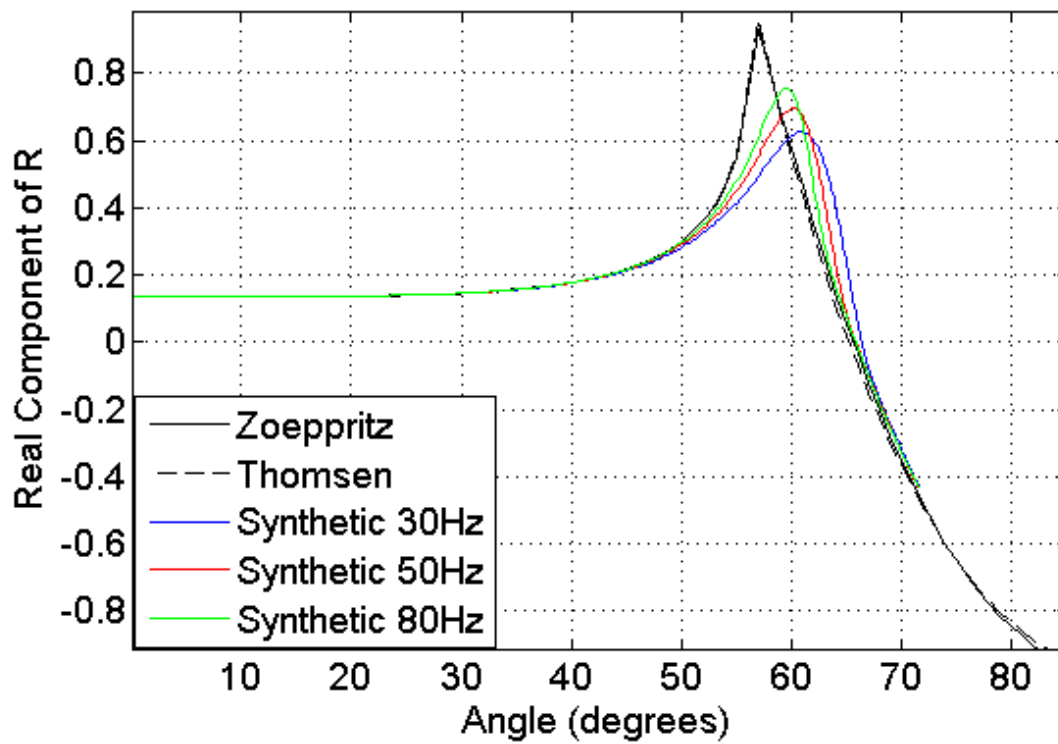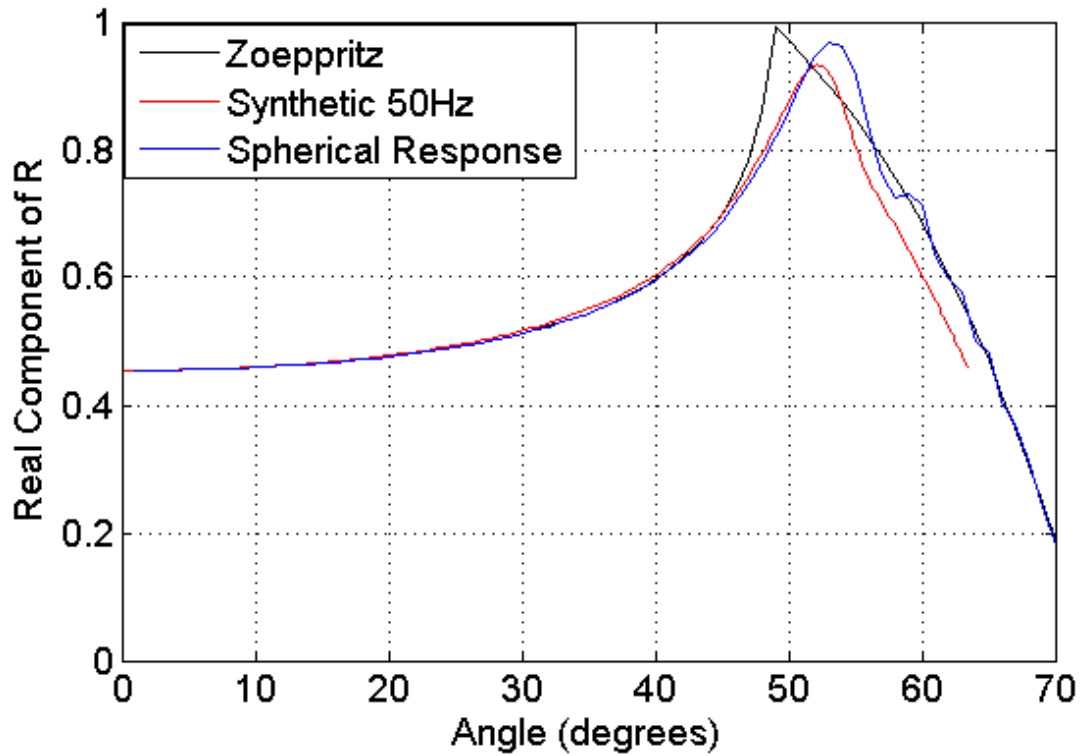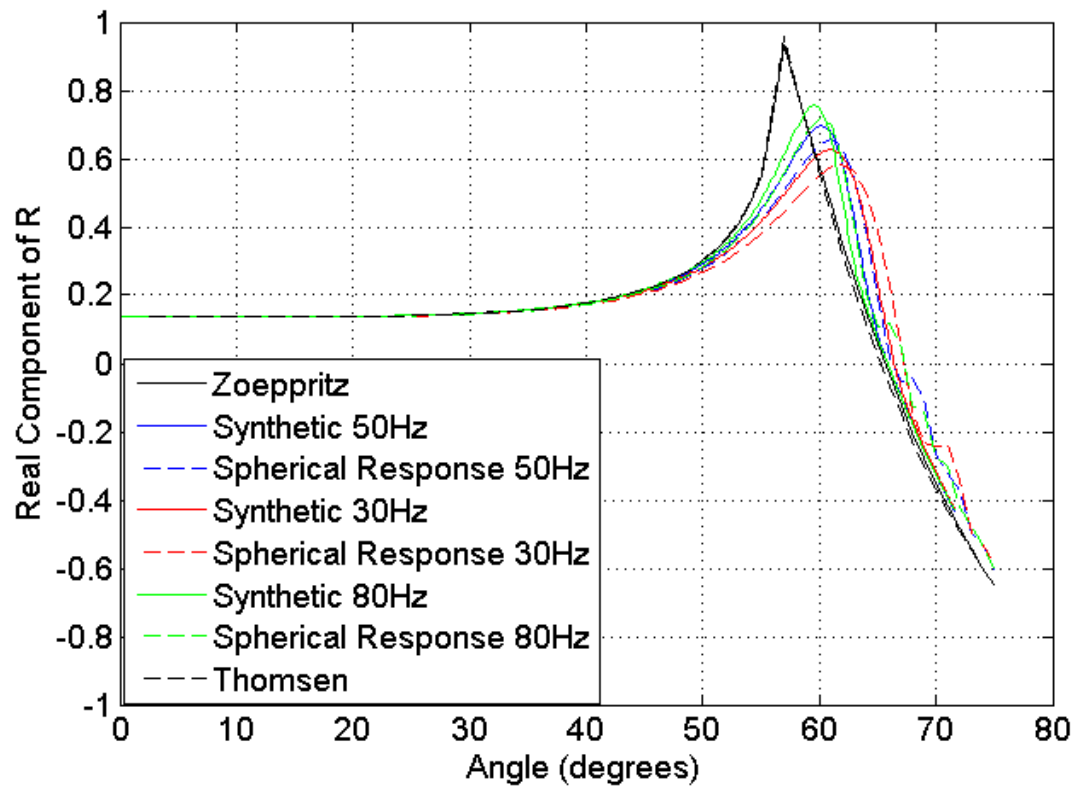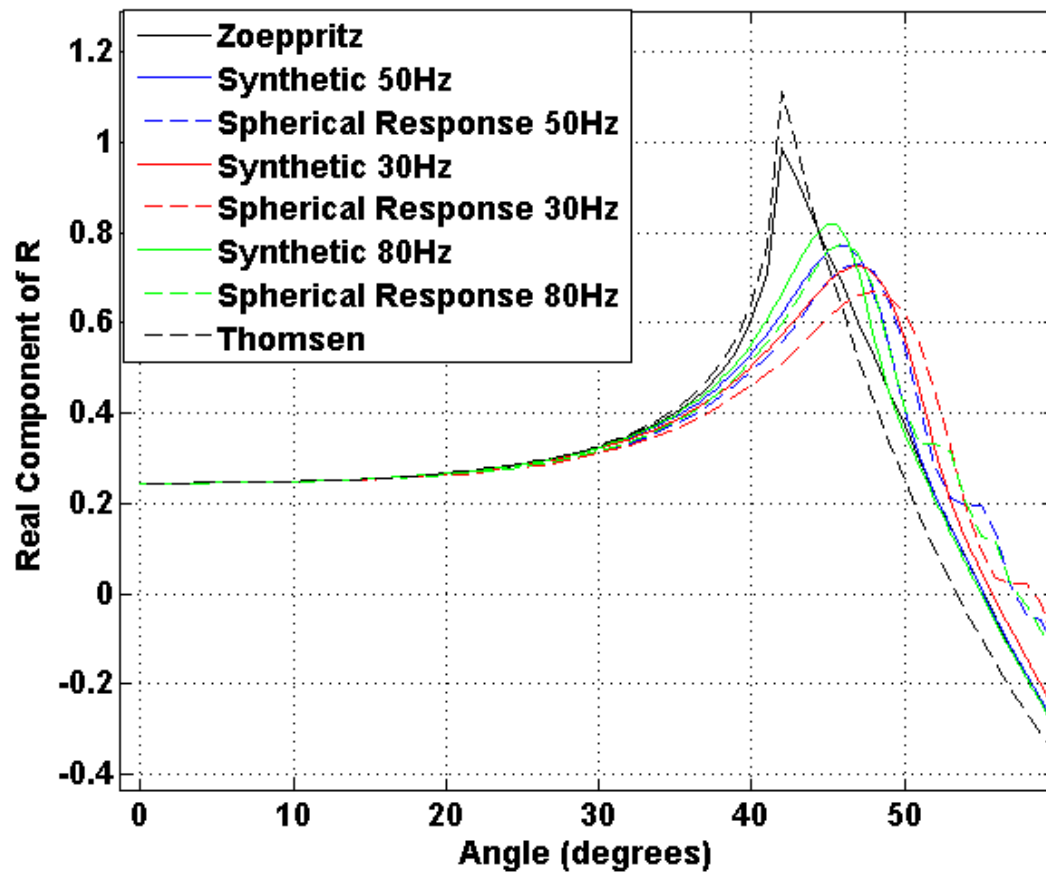
Figure 1. Real components of reflection coefficients computed using the Zoeppritz equations, Thomsen approximation and full elastic Model A with parameters shown in Table 1. Note the discrepancy in AVO response in the vicinity of critical angle. Also, note the frequency dependence of spherical wave responses.
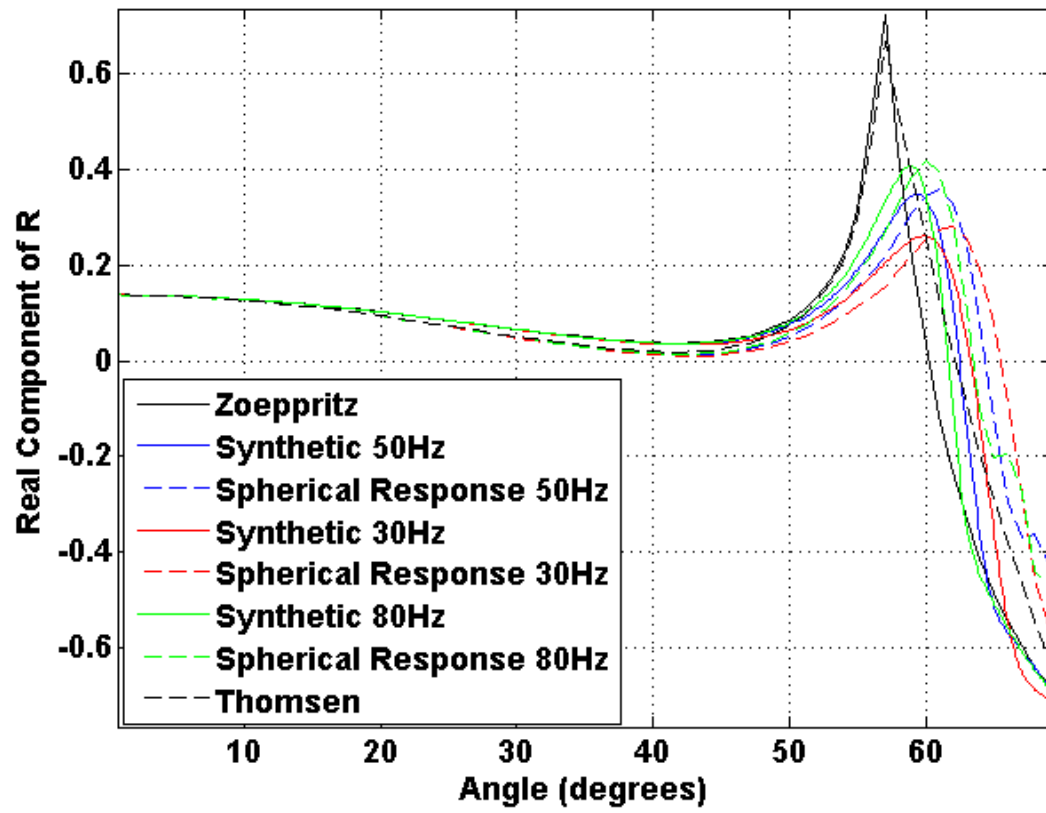

Figure 2. Comparison of real components of reflection coefficients computed from synthetic data (blue), Zoeppritz equations (black) and the spherical wave analytical solution at the fluid-fluid interface (red).

a)

Figure 3. Comparison of real components of reflection coefficients computed from synthetic data, and given by the Zoeppritz equations, Thomsen's linearised approximation, and the proposed spherical wave approximation at an interface between two media with parameters corresponding to Models A-I (Table 1).
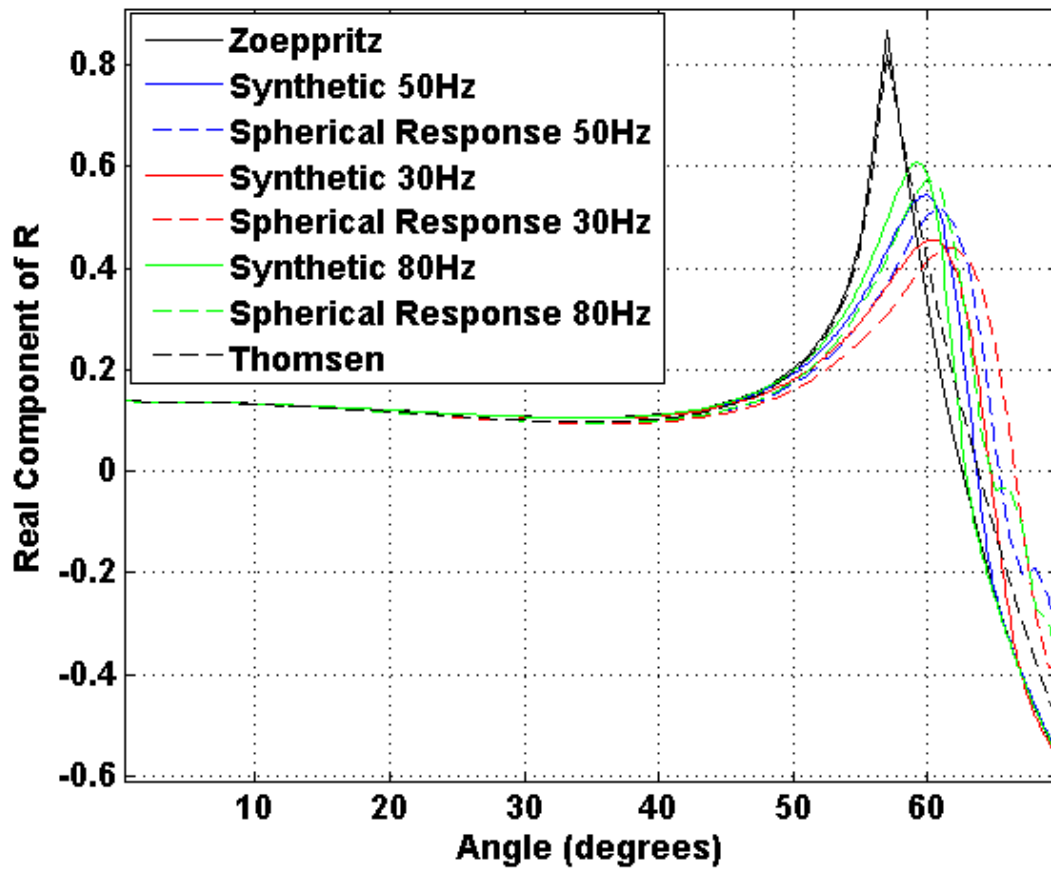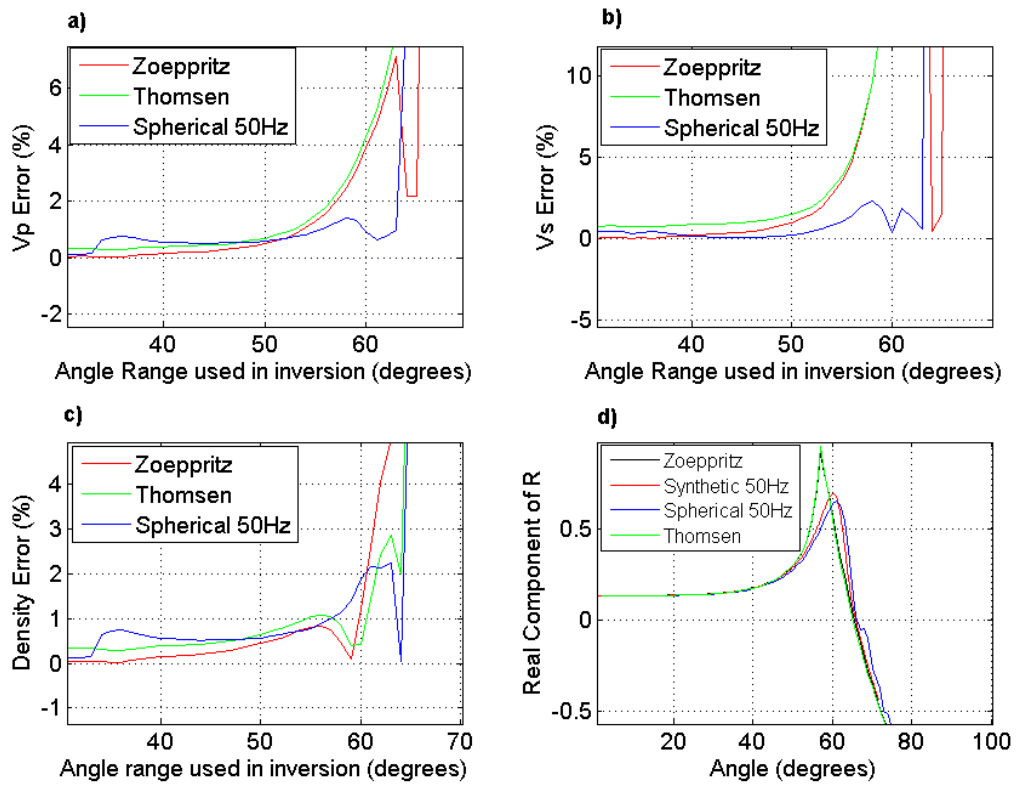
b)

c)

d)

Real Component of R vs Angle (degrees)

Legend:
- Zoeppritz
- Synthetic 50Hz
- Spherical Response 50Hz
- Synthetic 30Hz
- Spherical Response 30Hz
- Synthetic 80Hz
- Spherical Response 80Hz
- Thomsen

e)

f)

g)

h)

i)

Figure 4. Error in estimating V_{P2} (a), V_{S2} (b), and ρ_2 (c) in 3-parameter inversion of synthetic angle dependent reflectivity (d).
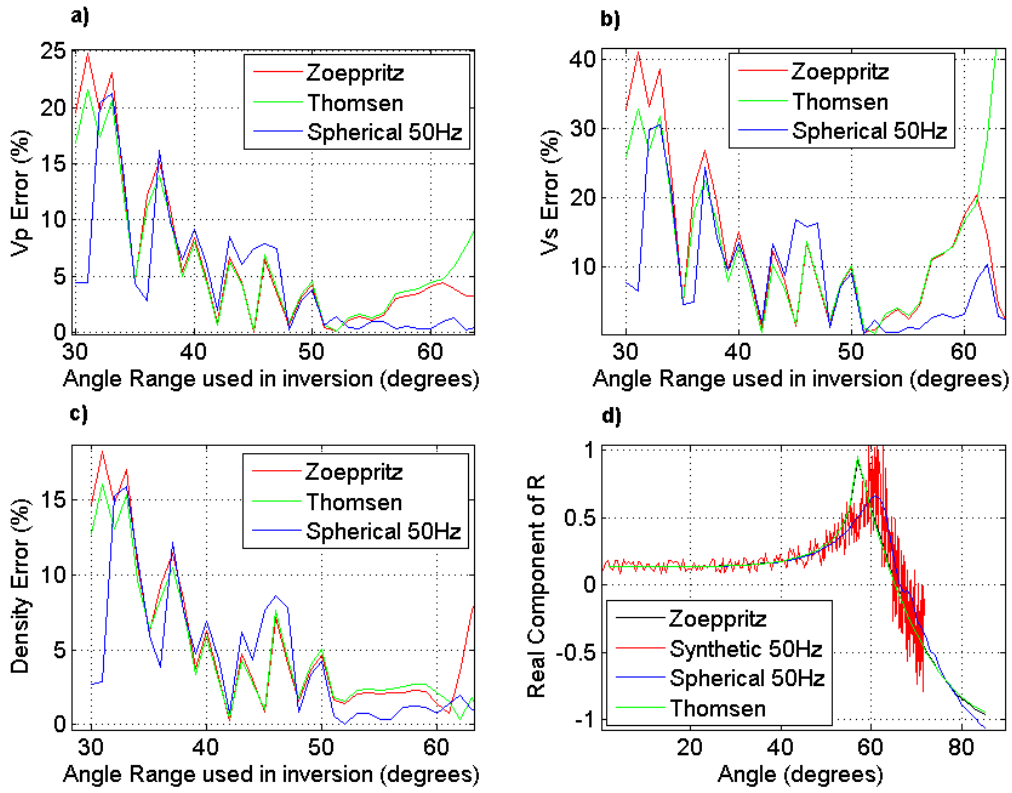
Figure 5. Error in estimating V_{P2} (a), V_{S2} (b), and ρ_2 (c) in 3-parameter inversion of synthetic angle dependent reflectivity with 50% added white noise (d).
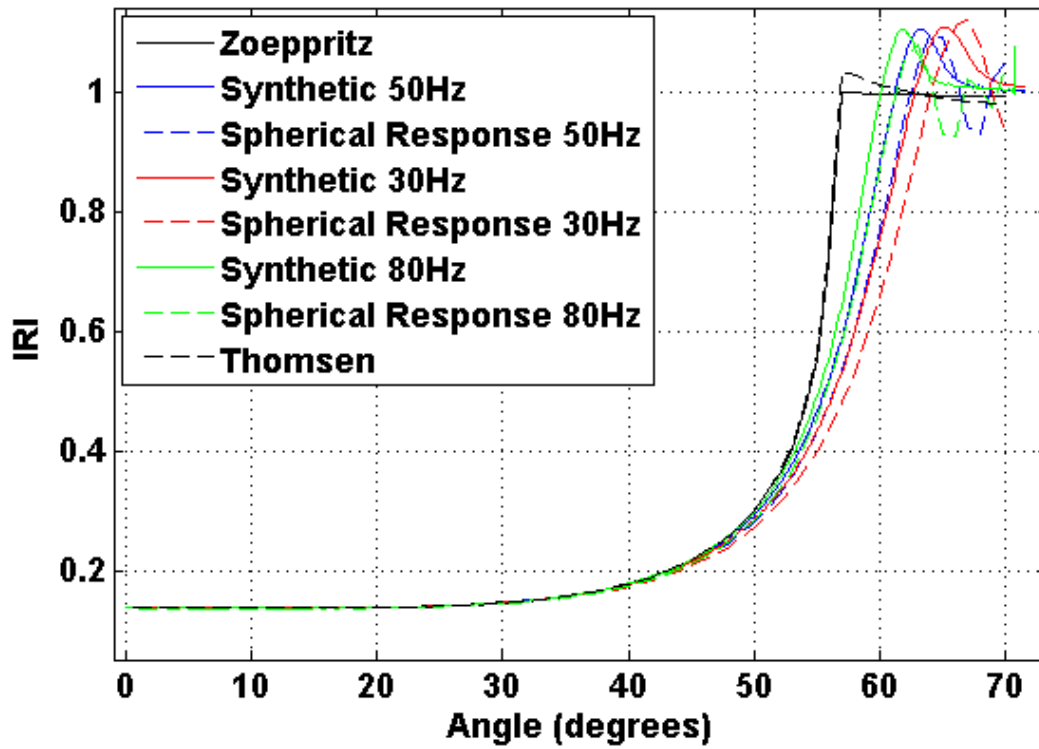
Figure 6. Same as Figure 3a but for absolute values of the reflection coefficients. 'Synthetic'

refers to amplitude of the envelope of the reflected wavelet.